Journal of Biomechanics 94 (2019) 138–146

Contents lists available at ScienceDirect

Journal of Biomechanics

journal homepage: www.elsevier.com/locate/jbiomech
www.JBiomech.com

Mechanical characterisation of human ascending aorta dissection

Valérie Deplano [a,*], Mourad Boufi [b,a], Vlad Gariboldi [c], Anderson D. Loundou [d], Xavier Benoit D'Journo [e], Jennifer Cautela [f], Amina Djemli [g], Yves S. Alimi [b]

[a] Aix Marseille Univ, CNRS, IRPHE, Ecole Centrale Marseille, Marseille, France
[b] Aix Marseille Univ, APHM, IFSTTAR, LBA, North Hospital, Department of Vascular Surgery, Marseille, France
[c] Aix Marseille Univ, APHM, Timone Hospital, Department of Cardiac Surgery, Marseille, France
[d] Aix Marseille Univ, SPMC EA3279, Department of Public Health, Marseille, France
[e] Aix Marseille Univ, APHM, North Hospital, Department of Thoracic Surgery, Marseille, France
[f] Aix Marseille Univ, APHM, North Hospital, Department of Cardiology, Marseille, France
[g] Aix Marseille Univ, APHM, North Hospital, Department of Pathology, Marseille, France

ARTICLE INFO

Article history:
Accepted 22 July 2019

Keywords:
Human ascending aorta
Acute type A dissection
Biaxial tensile test
In vivo measurements
Histological analysis

ABSTRACT

Mechanical characteristics of both the healthy ascending aorta and acute type A aortic dissection were investigated using *in vitro* biaxial tensile tests, *in vivo* measurements via transoesophageal echocardiography and histological characterisations. This combination of analysis at tissular, structural and microstructural levels highlighted the following: (*i*) a linear mechanical response for the dissected intimomedial flap and, conversely, nonlinear behaviour for both healthy and dissected ascending aorta; all showed anisotropy; (*ii*) a stiffer mechanical response in the longitudinal than in the circumferential direction for the healthy ascending aorta, consistent with the histological quantification of collagen and elastin fibre density; (*iii*) a link between dissection and ascending aorta stiffening, as revealed by biaxial tensile tests. This result was corroborated by *in vivo* measurements with stiffness index, β, and Peterson modulus, E_p, higher for patients with dissection than for control patients. It was consistent with histological analysis on dissected samples showing elastin fibre dislocations, reduced elastin density and increased collagen density. To our knowledge, this is the first study to report biaxial tensile tests on the dissected intimomedial flap and *in vivo* stiffness measurements of acute type A dissection in humans.

1. Introduction

An aortic dissection is a vascular pathology consisting in a tear of the aortic wall intima layer which can propagate downstream or/and upstream along the aorta, creating a false lumen through which blood flows. The Stanford classification divides aortic dissections into two types: type A when the initial tear is located along the ascending aorta and upstream of the left subclavian artery, and type B when the tear is located on the descending aorta. Acute type A dissection is characterised by rapidly developing severe complications such as aortic rupture, whereas chronic dissection is not diagnosed initially, being asymptomatic; patients remain stable. Acute type A dissection has a short- and long-term spontaneous mortality of 70% (Golledge and Eagle, 2008) and although its prognosis has been improved by surgical treatment, post-operative mortality remains high. The tear initiates when the aortic wall can no longer bear the wall stress exerted. While some biaxial tensile tests (Matsumoto et al., 2009; Haskett et al., 2010; Martin et al., 2011; Azadani et al., 2012; Kamenskiy et al., 2014), or pressurised tests (Labrosse et al., 2009) have been performed on healthy samples of human ascending aorta, there are few existing studies on dissected samples from acute type A dissection. To the authors' knowledge, only Babu et al. (2015) assessed mechanical properties of entire wall fragments from type A dissection. Studies using biaxial tensile or bulge inflation tests have generally focused on ascending thoracic aortic aneurysms (ATAA) (Okamoto et al., 2002; Pham et al., 2013; Duprey et al., 2016) rather than on dissection. Moreover, there have been few *in vivo* investigations of mechanical behaviour in dissections on the ascending aorta. Koullias et al. (2005) and Vitarelli et al. (2006) used echocardiography measurements to assess structural characteristics of ATAA and Marfan patients respectively. Shingu et al. (2009) were the only authors to use an echo-tracking system to obtain distensibility measurements, but on chronic dissection. Furthermore, the components of the extracellular matrix (ECM), their concentration and their organization are known to play an essential role in the mechanical behaviour of the human aorta (Tsamis et al., 2013).

* Corresponding author.
E-mail address: valerie.deplano@univ-amu.fr (V. Deplano).

https://doi.org/10.1016/j.jbiomech.2019.07.028
0021-9290/

Today, there is greater emphasis on quantifying the arterial microstructure and microarchitecture using, for example, microscopy image analysis (Koch et al., 2014) to corroborate macroscopic mechanical response and enrich constitutive laws and thus numerical modelling (Pasta et al., 2016; Thunes et al., 2018).

Here, we sought insights into the mechanical behaviour of the ascending aorta in acute type A dissection because of its high mortality risk. Three mechanical characterisations were therefore performed at different investigation levels. *In vivo* measurements were performed on both healthy and pathological patients to obtain results at structure level. These measurements were combined with appropriate *in vitro* biaxial tensile tests on both healthy and dissected aortic samples to assess information at tissular level. Finally, qualitative and quantitative histological analyses were carried out on both types of samples to link structural, tissular and microstructural level.

2. Methods

2.1. Tissue preparation

Healthy ascending aorta, *Haa*, tubular structures were harvested from unused aortic segments after lung transplantation. Dissected ascending aorta, *Daa*, fragments were collected from patients after surgical repair. Informed consent was obtained based on established research board protocol in each hospital. All samples were stored, refrigerated at 4 °C in 0.9% NaCl solution and tested less than 50 h after tissue extraction.

The *Haa* tubular structures (Fig. 1a) were longitudinally cut along the curvature. Three types of samples were extracted from dissected fragments (Fig. 1b): a region without dissected layers, *WDaaL*, n = 1, (Fig. 1d), the adventitia layer alone, n = 3, (Fig. 1e), and the media associated with the intima layer called intimomedial flap, n = 3, (Fig. 1f). Square 20X20mm samples (a reproducible size) were subsequently obtained from healthy and dissected samples, using a dedicated cutting device. Seven healthy samples from 5 different donors of mean age 65.3 ± 4.9 years, with a mean thickness of 2.26 ± 0.19 mm, were tested. The mean thickness and patient mean age of the flap and adventitia samples were 1.98 ± 0.12 mm; 63.7 ± 9.2 years and 1.06 ± 0.17 mm; 59.7 ± 8.3 years respectively. The thickness of *WDaaL* was 1.79 mm and the patient was 57 years old. Thickness was measured via image processing of the undeformed samples (Deplano et al., 2016). Table A.1Appendix A reported demographic data and risk factors of all *in vitro* tested samples.

2.2. In vitro mechanical tests

The square samples were mounted using a home-made biaxial set-up described in Deplano et al. (2016). Briefly, the circumferential, θ, and longitudinal, L, directions of the sample were in line with the biaxial displacements. A displacement-driven protocol was applied while the ratio, α, remained constant. $\alpha = \frac{\lambda_\theta}{\lambda_L}$, noted $\alpha = \lambda_\theta : \lambda_L$, was the stretch ratio, λ_θ and λ_L being the stretch in the θ, and L directions respectively.

Forces resulting from the displacements were measured using two load cells (10 N ± 0.0015 N, 31E10, Honeywell) located on each direction of displacement. 3D displacement measurements (Dantec Q-400 software) were performed using Stereoscopic Digital Image Correlation. Samples were submerged in aqueous 0.9% NaCl solution maintained at 37 °C during the experiments.

The maximum stretch, λ_{max}, was set at 1.2 of the gripped undeformed sample area, $X_L \times X_\theta$, where $X_L = X_\theta = 18$ mm were measured before the protocol was applied. Twenty loading and unloading cycles of preconditioning were first performed at λ_{max} and $\alpha = 1:1$ following by k = 7 consecutive cycles, each one at different stretch ratios: 0.75:1, 1:0.75, 0.5:1, 1:0.5, 0.25:1, 1:0.25, 1:1. This protocol was applied for a maximum stretch rate of $\dot{\lambda}_{max} = 3.84 \times 10^{-2}\ s^{-1}$. Initial zero stress was assessed by tuning the position of the suture lines by 0.1 mm steps at a very low displacement rate (0.1 mm/s) until the load cell signals detected were above their noise level (2.4 mV). A hybrid displacement/force control was implemented during unloading to avoid bending the sample with respect to its original dimensions.

The first Piola Kirchhoff stress tensor, P, was determined using f_θ and f_L, the recorded force, $X_\theta^{k-1}, X_L^{k-1}$ and E_0, the undeformed gripped sample dimensions and thickness. For each cycle

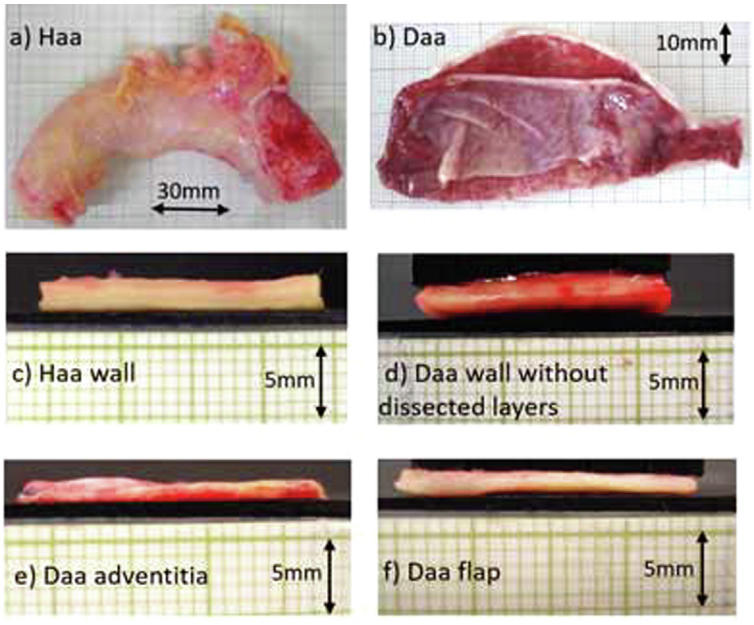

Fig. 1. (a) Representative healthy human ascending aorta, *Haa*. (b) Representative fragment of dissected aorta, *Daa*. Side view of representative wall thickness of (c) *Haa*, (d) *Daa* without dissected layers, (e) adventicia layer of *Daa*, (f) intimomedial flap of *Daa*.

performed during one protocol, X_θ^{k-1} and X_L^{k-1} correspond to the undeformed lengths of the sample at the end of the k − 1 unloading path.

The components of P were expressed by $P_{\theta\theta}^k = \frac{f_\theta}{X_L^{k-1} E_0}$ and $P_{LL}^k = \frac{f_L}{X_\theta^{k-1} E_0}$. The components of the second Piola Kirchhoff stress tensor, S, were then obtained using $S_{\theta\theta}^k = \frac{P_{\theta\theta}^k}{\lambda_\theta}$ and $S_{LL}^k = \frac{P_{LL}^k}{\lambda_L}$, those of the Cauchy stress tensor, σ, using: $\sigma_{\theta\theta}^k = P_{\theta\theta}^k \lambda_\theta$ and $\sigma_{LL}^k = P_{LL}^k \lambda_L$. λ_i were calculated from the SDIC displacement measurements. The superscript k will be omitted in the rest of the paper.

2.3. Histological characterisation

Healthy and dissected segments (n = 3 and n = 4 respectively) were first fixed in 10% formalin (Appendix A details their characteristics). For each sample, 2 contiguous samples were cut along the axial and transversal artery axis. They were dehydrated in ethanol and embedded in paraffin. Four contiguous sections 5 µm thick were cut and stained with orceid and Trichrome masson for the visualisation of elastin and collagen fibres respectively. Calopix software was then used for image processing and extraction of the relative density of the stained structures. Density was defined as the ratio of stained surface to total surface for a region of interest of the sample. For each sample, density was measured in 4 regions in media layers and in the entire wall, and averages were calculated.

2.4. In vivo measurements

To determine the mechanical behaviour of both healthy and dissected ascending aorta, *in vivo* transoesophageal echocardiography measurements were performed on two new groups of patients not used for the *in vitro* tests and histological characterisations. The control group (n = 22, age 67 ± 9 years, 19 males) was composed of patients without any ascending aorta pathology, while the second group (n = 13, age 69 ± 10 years, 9 males) was composed of patients admitted and treated for acute type A dissection. The mechanical characterisation of both groups entailed determining the Peterson modulus, E_p, and stiffness index, β. $E_p = \frac{\Delta P}{\epsilon}, \beta = \frac{\ln \frac{P_{sys}}{P_{dias}}}{\epsilon}$, where $\epsilon = \frac{\Delta D}{D_{dias}}$, ΔP and ΔD were the difference between the diastolic and systolic pressure (P_{dias}, P_{sys}) and diameter (D_{dias}, D_{sys}) values respectively. Details of pressure and diameter acquisitions as well as inclusion criteria for each group are given in Appendix B.

3. Results

3.1. Constitutive modelling

Fig. 2(a)–(d), which represent $S - \lambda$ curves for both *Haa* and *WDaaL* samples, show nonlinear and rather anisotropic behaviour. These mechanical responses were therefore modelled by a Holzapfel-Gasser-Ogden (HGO) form of strain energy function, ψ, as per Babu et al. (2015).

$$\psi = \psi_{iso} + \psi_{aniso} \quad \text{with} \quad \psi_{iso} = \frac{C}{2}(I_1 - 3) \quad \text{and} \quad \psi_{aniso} = \frac{k_1}{k_2}\left(e^{\left(k_2 (I_4 - 1)^2\right)} - 1\right)$$

considering that collagen fibres are symmetrically oriented in the arterial wall. C and k_1 are positive dimensional (Pa) coefficients and k_2 is dimensionless. I_1 is the first invariant of the strain tensor and $I_4 = \lambda_\theta^2 \cos^2\gamma + \lambda_L^2 \sin^2\gamma$, where γ is the angle between the fibre direction and the circumferential direction.

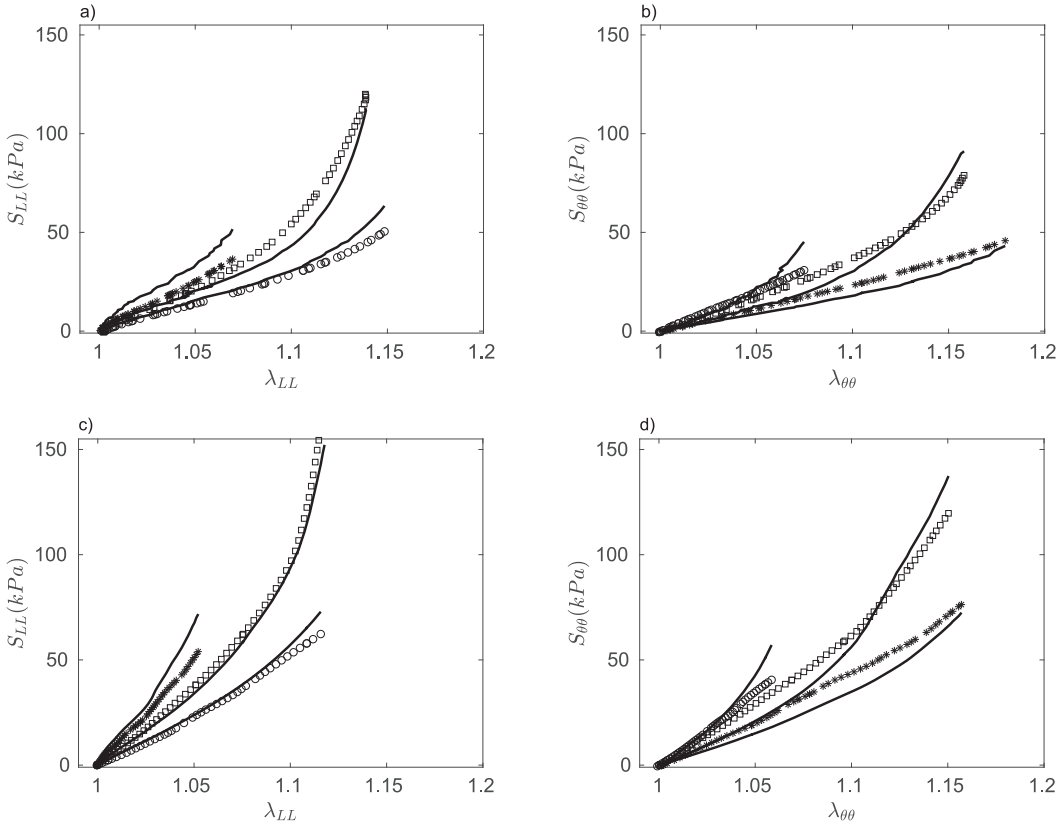

Fig. 2. S-λ curves. (a) & (b) Mean data obtained from *Haa* samples. (c) & (d) *Daa* wall without dissected layers. $\alpha = 0.5$ (circle symbol), $\alpha = 2$ (star symbol) and $\alpha = 1$ (square symbol). Symbols are used for experimental data and solid lines for constitutive modelling. (a) and (c): L direction. (b) and (d): θ direction.

Fig. 3(a) and (b), which show $S-E$ curves for the *Daa* intimomedial flap, highlight more or less linear and anisotropic behaviour. According to these results, the mechanical response was described by a 3-parameter polynomial strain energy function, $\psi = \frac{1}{2}\left(A_{\theta\theta}E_{\theta\theta}^2 + 2A_{\theta L}E_{\theta\theta}E_{LL} + A_{LL}E_{LL}^2\right)$. $E_{\theta\theta}$ and E_{LL} are the components of the Green-Lagrangian strain tensor. The coefficients $A_{\theta\theta}$ and A_{LL} describe the tissue stiffness in the θ and L directions respectively and $A_{\theta L}$ is related to the interaction between the two directions.

Whatever the constitutive modelling, the components of the second Piola Kirchhoff stress tensor can be derived from ψ according to $S = \frac{\partial\psi}{\partial E}$. The coefficients C, k_1, k_2 and γ angle for the HGO model, and $A_{\theta\theta}$, A_{LL} and $A_{\theta L}$ for the linear model were thus obtained using an optimization procedure (using fmincon function in Matlab). Part of the mechanical data from the biaxial protocol was simultaneously fitted to the constitutive model. For *Haa* and *WDaaL*, mechanical data from α = 0.5:1;1:0.5, and 1:1 were used. For the *Daa* flap, mechanical data from α = 0.75:1; 1:0.75, 0.5:1, 1:0.5 were considered.

The method involved minimizing the sum of the error χ_α (Eq. (1)), e.g. $\sum_\alpha \chi_\alpha$ where α was the stretch ratio and m the number of experimental data recorded during loading (e.g m = 60).

$$\chi_\alpha = \sum_{k=1}^{m}\left(S_{\theta\theta}^{exp} - S_{\theta\theta}^{mod}\right)_k^2 + \left(S_{LL}^{exp} - S_{LL}^{mod}\right)_k^2 \quad (1)$$

The superscript *exp* indicates the stress values from the experimental data, *mod* those predicted by the model.

Table C.1 Appendix C displays the C, k_1, k_2 coefficients and γ angle for the mean data obtained from the healthy samples (n = 7) and for the single *WDaaL* sample tested. Table C.2 Appendix C presents the A_{ij} coefficients obtained through the optimization procedure for each *Daa* flap sample and the mean data obtained from all flap samples. For each constitutive modelling process, the coefficients obtained at the end of optimization procedures converged towards the same values, whatever the initial guesses tested.

For mean data obtained from *Haa* samples and *WDaaL* data, the stress components derived from the strain energy function fitted the experimental data with average determination coefficients $\overline{R_L^2}$ of 0.811 and 0.911 respectively and $\overline{R_\theta^2}$ of 0.861 and 0.902 respectively (Table C.1 Appendix C). For mean data obtained from the flap samples, we found $\overline{R^2}$ of 0.991 and 0.995 in the longitudinal and circumferential direction respectively (Table C.2 Appendix C). Fig. 3(a) and (b) underline the good fit between experimental data and constitutive modelling for flap mean data. This is further illustrated by Fig. 4(a) and (b), which show that the model's prediction of $S-E$ behaviour for $\alpha = 1$ is very close to the experimental behaviour, even though this latter dataset was not used in the identification procedure.

3.2. Mechanical behavior of healthy and dissected ascending aorta

3.2.1. In vitro mechanical tests

None of the tensile tests performed on the adventitia *Daa* samples could be exploited, due to systematic tearing under stress.

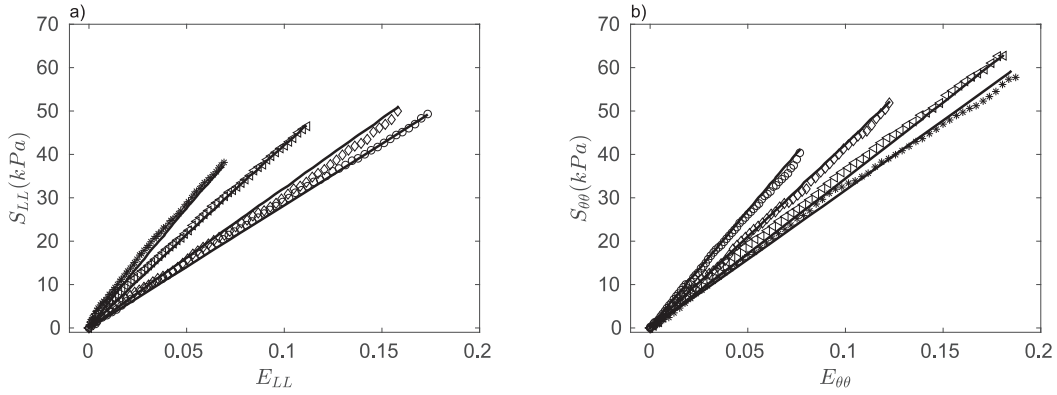

Fig. 3. S-E curves plotted for the mean data obtained from the *Daa* intimomedial flap samples. α = 0.75, 1.33, 0.5, and 2 (diamond, triangle, circle and star symbols respectively). Symbols are used for experimental data and solid lines for constitutive modelling. (a) L direction. (b) θ direction.

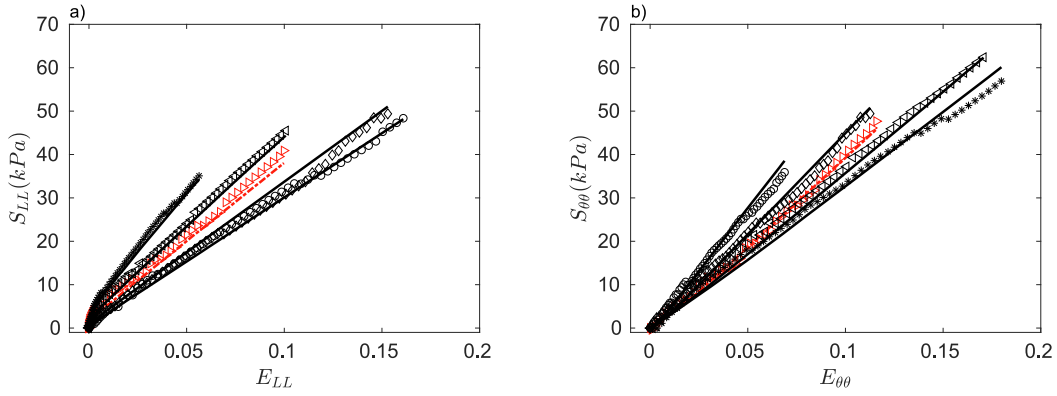

Fig. 4. S-E curves illustrating a *Daa* intimomedial flap sample for α = 0.75, 1.33, 0.5, and 2 (diamond, triangle, circle and star symbols respectively). Symbols are used for experimental data and solid lines for constitutive modelling. Red curves are for α = 1 that were not used for parameters identification. (a) L direction. (b) θ direction. (For interpretation of the references to colour in this figure legend, the reader is referred to the web version of this article.)

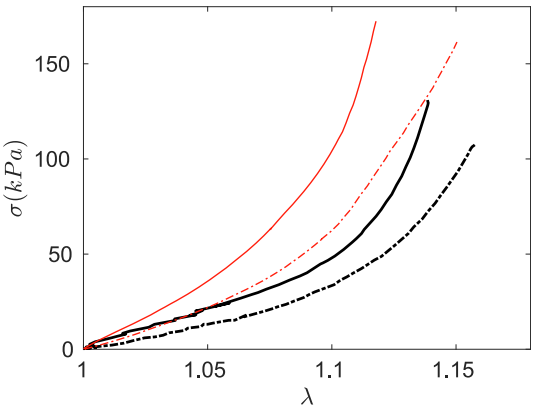

Fig. 5. Comparison of $\sigma - \lambda$ curves between *Daa* wall without dissected layers sample and *Haa* mean sample (red thin and black thick lines respectively). Curves are plotted using constitutive modelling and $\alpha = 1$. Solid and dashed lines are used for the L and θ direction respectively. (For interpretation of the references to colour in this figure legend, the reader is referred to the web version of this article.)

To compare the mechanical behaviour of *Haa* with that of *WDaaL*, $\sigma - \lambda$ curves for $\alpha = 1$ in both longitudinal and circumferential directions were plotted using an HGO model (Fig. 5). As mentioned, both samples exhibited nonlinear and anisotropic behaviour. The mechanical response of *WDaaL* was stiffer than that of *Haa* and both their responses were stiffer in the longitudinal than in the circumferential direction. Although rather linear, the mechanical behaviour of *Daa* flap samples (Fig. 3(a) and (b)) was also anisotropic; however their $A_{\theta\theta}$ coefficient was greater than A_{LL} one, 277.653 versus 232.861 kPa, (Table C.2 Appendix C).

To compare anisotropy characteristics of *Haa* and *WDaaL*, stress levels at 80 mmHg and 120 mmHg were first computed using Laplace law $\sigma_\theta = \frac{Pr}{h}$; P and r being P_{dias} and $\frac{D_{dias}}{2}$ or P_{sys} and $\frac{D_{sys}}{2}$ respectively (Table 2); h being the wall thickness. Using the experimental $\sigma - \lambda$ curves, values of longitudinal and circumferential stretches were then inferred for σ_θ Laplace values at 80 and 120 mmHg using interpolation. The assessment of anisotropy at diastole, Ani_{80}, and systole, Ani_{120} were then defined (Kamenskiy et al., 2014) as the difference in longitudinal and circumferential stretches divided by their average value. Whatever the stress level considered, the negative anisotropy values confirm that mechanical response is stiffer in the longitudinal direction for both healthy and *WDaaL* samples (Table C.1 Appendix C). Moreover, these high values show that anisotropy increases when there is dissection, $Ani_{80} = -0.017$, $Ani_{120} = -0.03$ for *Haa* versus -0.025 and -0.037 respectively for *WDaaL*. Finally, for *Daa* flap samples the mean anisotropic level, defined as $Ani = 2\frac{A_{LL} - A_{\theta\theta}}{A_{LL} + A_{\theta\theta}}$, is 0.175 (Table C.2 Appendix C). While *Haa* and *WDaaL* show a stiffer response in the longitudinal direction, flap samples behave in the opposite way.

3.2.2. Histological characterisation

Figs. 6 and 7 illustrate histological transversal and axial cuts of *Haa* and *Daa* flap samples respectively. A sketch of both cuts (Fig. 6e) shows that the transversal cut (TC) and axial cut (AC) generate faces that will be stretched in the longitudinal and circumferential direction respectively. Observations of the *Haa* TC reveal less

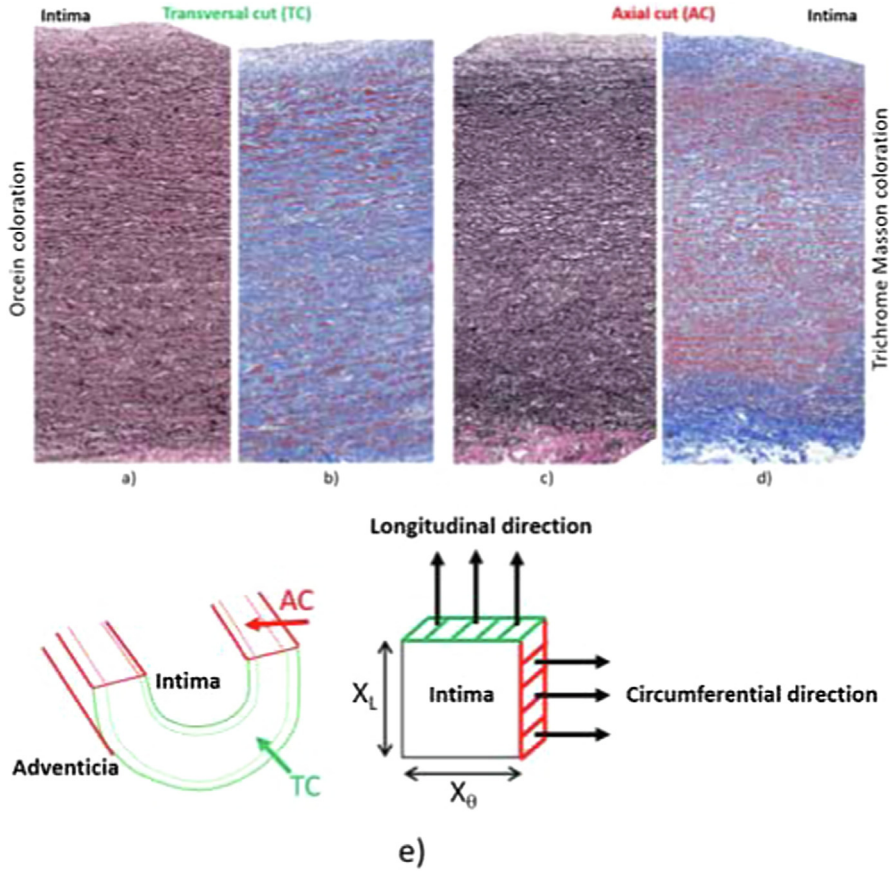

Fig. 6. Transversal (a and b) and axial (c and d) histological cuts of *Haa*. Elastin fibres are colored in black (a) and (c) (orceid staining). Collagen fibres are colored in blue (b) and (d) (Trichrome masson staining). (e) Scheme of arterial cuts and their corresponding stretching directions. (For interpretation of the references to colour in this figure legend, the reader is referred to the web version of this article.)

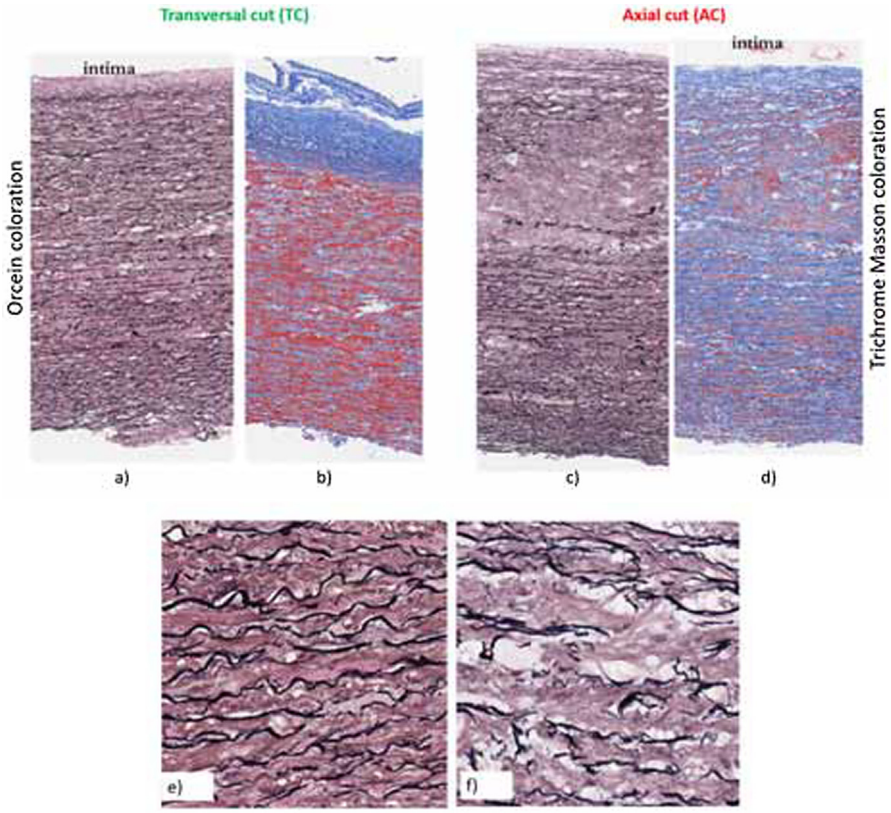

Fig. 7. Transversal and axial histological cuts of *Daa* flap. Elastin fibres are colored in black (a) and (c) (orceid staining). Collagen fibres are colored in blue (b) and (d) (Trichrome masson staining). Zoom of the media layer histological transversal cut stained with orceid. (e) Haa, (f) Daa flap. (For interpretation of the references to colour in this figure legend, the reader is referred to the web version of this article.)

Table 1
Average values in % of the elastin and collagen fibres areal density for both healthy and dissected samples.

fibres	Healthy samples		Dissected samples	
	n = 3		n = 4	
	Axial cut	Transversal cut	Axial cut	Transversal cut
		Within total wall		
Elastin (%)	30 ± 5.5	19.5 ± 3	NA	NA
Collagen (%)	50.5 ± 4	70.5 ± 14	NA	NA
		Within media layer		
Elastin (%)	30 ± 6	18 ± 2	20 ± 2	24 ± 3.5
Collagen (%)	54 ± 4	66 ± 8	60 ± 4.5	45 ± 6

elastin and more collagen fibres than for the AC (Fig. 6(a), (b) and (c), (d) respectively). The fibre areal densities (Table 1) quantitatively confirm these qualitative data. The ratio of collagen to elastic areal density within the *Haa* TC total wall is greater than for AC, 3.61 versus 1.68.

Qualitative and quantitative comparison of histological cuts of *Haa* and dissected samples (Figs. 6, 7 and Table 1) highlights lower elastin fibre density and higher collagen fibre density for the dissected samples within the AC of the media layer compared to healthy samples (20 ± 2 versus 30 ± 6 and 60 ± 4.5 versus 54 ± 4 respectively). Moreover, Fig. 7(b) and (a) clearly show areas with broken elastin fibres and dislocations, when flap media are compared with *Haa* media.

3.2.3. In vivo measurements

Comparison of E_p and β parameters (Table 2) between the two groups of patients shows that those with dissection have a significantly higher stiffness index than control patients, with 20.7 ± 24 versus 6.1 ± 2.8, p = 0.013. In addition, mean E_p in the dissection group is 436 ± 393 kPa, compared to 198 ± 107 kPa in the control group (p = 0.041).

The systolic and diastolic aortic diameters are significantly larger in the dissection group (p < 0.001 for both) and no correlation is found between systolic ascending aorta diameter and stiffness index (p = 0.87) and E_p (p = 0.82).

4. Discussion and conclusion

The first question that merits discussion is whether the behaviour of the healthy aortic ascending wall is anisotropic or isotropic. This suggests the need to link analyses performed at different scales to enhance understanding. Results in the literature differ depending on the donors' age. Azadani et al. (2012) and Martin et al. (2011) showed isotropic behaviour for both relatively young (mean age

Table 2
Systolic and diastolic diameter and pressure values from *in vivo* measurements. Resulting Peterson modulus and stiffness index values for control and dissection groups. Data were expressed as mean ± standard deviation. Comparisons were performed using the Mann-Whitney U test. The statistical significance was defined as $p < 0.05$

	Control group (n = 22)	Dissection group (n = 13)	p
Systolic diameter (mm)	34.8 ± 4.9	47.7 ± 5.5	<0.001
Diastolic diameter (mm)	33.4 ± 4.9	44.3 ± 5.2	<0.001
Systolic pressure (mmHg)	137 ± 25	110 ± 22	0.06
Diastolic pressure (mmHg)	79 ± 14	57 ± 17	0.01
E_p (kPa)	198 ± 107	436 ± 393	0.041
β	6.1 ± 2.8	20.7 ± 24	0.013

47) and very old (aged from 81 to 98) donors. Labrosse et al. (2009) and Haskett et al. (2010) observed anisotropic behaviour with a stiffer mechanical response in the circumferential direction than in the longitudinal direction for patients aged from 31 to 71. However, Haskett et al. (2010) also observed that the longitudinal direction tended to stiffen with age more than the circumferential direction, with donors over 61 showing lower longitudinal than circumferential peak strain. In addition, Kamenskiy et al. (2014) reported that 7 patients out of 8, with a mean age of 54, had a more compliant mechanical response in the circumferential direction than longitudinally. The general mechanical behaviour of our donors, 58–69 years old, nonlinear and anisotropic, is consistent with behaviours observed in the literature for the same age (Fig. 8). In our case, the mechanical response is stiffer in the longitudinal direction. In parallel, the ratio of collagen to elastic areal density is greater for a sample face stretched in the longitudinal direction. As collagen fibres contribute to stiffening whereas elastic fibres increase distensibility, the histological analysis confirms the results obtained using biaxial tensile tests.

Several components of the extra-cellular matrix may be involved in dissection and the associated mechanisms are not yet fully understood. Dysfunction in the contractile apparatus within smooth muscle cells may place the thoracic aorta at increased risk (Emmott et al., 2016). Humphrey (2013) or Roccabianca et al. (2017) have, meanwhile, revealed that pooled glysaminoglycans/proteoglycans can induce stress concentration and pressure swelling within the aortic wall, and thus contribute to dissection. Nevertheless, elastin and collagen fibres are obviously implicated in arterial wall elasticity, tensile stiffness and strength, and anisotropy with stiffer mechanical response in the longitudinal direction could also play a role in dissection.

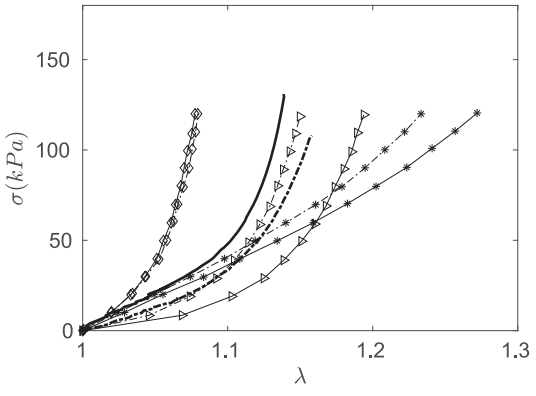

Fig. 8. Comparison of $\sigma - \lambda$ curves between mean values of our *Haa* samples (without symbol) and *Haa* of literature (diamond, triangle and star symbols for Martin et al. (2011), Labrosse et al. (2009) and Haskett et al. (2010) respectively; extracted from (Roccabianca et al., 2014)). Our curves are plotted using constitutive modelling and $\alpha = 1$. Solid and dashed lines are used for the L and θ direction respectively.

Few mechanical characterisations have been performed on dissected ascending aortic walls; it is therefore important to compare healthy and dissected samples. Like *Haa*, *WdaaL* presents a stiffer mechanical response in the longitudinal direction. Although the number of samples we tested is a limitation, this result is in agreement with the only published work using biaxial tests to characterise the mechanical behaviour of *WDaaL*: Babu et al. (2015) observed the same anisotropic feature for patients over 50 years old with a dissection. Complementarity between *in vitro* and *in vivo* measurements, a strength of our method, enables us to further the analysis. By subjecting excised aorta samples to mechanical solicitation via *in vitro* biaxial tensile tests, anisotropy, nonlinearity and stress are assessed at different stretch values; Young's modulus can also be inferred within a specific range of solicitations. *In vivo* measurements enable aorta radial strain and pressure to be assessed at systolic and diastolic instants, thereby revealing aorta distensibility (β or E_p). These two supplementary measurements allow arterial stiffness to be assessed from a different perspective. Here, *WDaaL* showed greater rigidity than *Haa*. Only one *WdaaL* was tested, but this *in vitro* assessment is confirmed by *in vivo* measurements performed on 13 patients with dissection and 22 without. Patients with dissection had a significantly higher stiffness index and E_p values than control. Moreover, as the *in vivo* measurements were performed on patients of comparable ages, the dissection stiffening cannot solely be associated with ageing. The relevance of our *in vivo* measurements is underlined by the fact that we found a mean E_p value in the control group, consistent with the literature values based on normal populations similar to ours in age and vascular risk factors (Hirata et al., 1991 and Stefanadis et al., 1990).

Moreover, *in vivo* measurements can challenge assumptions in the clinical indexes used to evaluate dissection risk. The aortic diameter is often considered an important parameter to assess dissection evolution. Here, although both systolic and diastolic diameters were significantly larger in the dissection group, no correlation appears between systolic diameter and β or E_p. As dissection is clearly associated with stiffening, diameter does not therefore appear to be relevant to predict the evolution of dissection.

More work should be focused on better evaluating dissection evolution risk. Not only is there a lack of mechanical characterisations of dissected aorta samples, but there is also a pressing need to couple such studies with microstructural analysis, so as to link overall mechanical response to microstructural modification and focus on local changes in wall integrity.

Furthermore, fluid structure numerical modelling can add important information on the quantification of hemodynamic loads at the wall and which are thus transmitted/perceived by the arterial wall cells. To date, few numerical studies have used FSI modelling and appropriate arterial wall constitutive laws (Alimohammadi et al., 2016). The results obtained in this work on flap and dissected ascending aorta wall stiffness could be used to perform such FSI numerical simulations, thereby contributing to the understanding of hemodynamic stimuli. This would improve modelling of the aortic cell response to such hemodynamic solicitations.

To conclude, this work used *in vitro* biaxial tensile tests, *in vivo* measurements via transoesophageal echocardiography and histological characterisation for ascending aorta mechanical

characterisation, thereby combining tissular, structural and microstructural levels in an original approach. To our knowledge, this is the first study reporting biaxial tensile tests on the intimomedial flap, and our *in vivo* investigations of mechanical properties on acute type A dissection are the first in humans. Our major findings are: (*i*) The mechanical response of the intimomedial flap shows linear behaviour up to stretch values of 1.2. Conversely, *Haa* and *WDaaL* behave in a nonlinear way. However, all show anisotropy. (*ii*) The mechanical response of *Haa* in the longitudinal direction is stiffer than in the circumferential direction. (*iii*) Dissection promotes ascending aorta stiffening.

The present work has some limitations. A larger number of samples would be preferable, especially for biaxial tensile tests; we were mainly limited by the logistics of testing fresh tissue. The tensile test protocol was established in such a way as to be relevant to both healthy and dissected samples. In particular, a rather low value of λ_{max} = 1.2 was chosen to test the dissected adventitia layer because of its fragility. Unfortunately, we did not manage to test this specific sample, which would have permitted us to increase λ_{max} for the other mechanical tests. Finally, the quantitative analysis of collagen results contained in the histomorphetric data should be considered with caution, because of the nonspecific nature of Trichrome Masson staining. Despite these limitations, which are currently the subject of ongoing studies, our combination of *in vitro*, *in vivo* and histological results provides new insights into the mechanical characteristics associated with ascending aorta dissection.

Declaration of Competing Interest

All authors declare that there are no conflict of interest.

Acknowledgment

The authors thank the Labex MEC ANR-11-LABX-0092 for financial support. We thank Marjorie Sweetko for English language revision.

Appendix A. Table of subject characteristics

Table A.1 details the subject characteristics of all the samples tested using the biaxial tensile set-up.

The number of healthy samples (n = 3) histologically characterised, was a subset of those tested on the biaxial tensile device. Two out of four dissected samples, which have been histologically characterised, were also tested on the biaxial tensile device. The 2 dissected samples, that were not tested *in vitro*, came from patients with similar risk factors as those tested.

Table A.1
Donors and dissected subject characteristics. M for male, F for female, HBP for High Blood Pressure.

Donor(D) ID and Sample(S) ID	Age(yr)	Gender	Risk factors (Rf)
D1S1	69	M	HBP
D2S1, D2S2, D2S3	69	M	No Rf
D3S1	58	M	Smoking
D4S1	59	F	No Rf
D5S1	64	M	HBP and smoking
Flap(F) ID and Sample(S) ID	**Age(yr)**	**Gender**	**Risk factors**
F1S1, F1S2	69	M	HBP
F2S1	53	M	No Rf
WDaaL(W) ID and Sample(S) ID	**Age(yr)**	**Gender**	**Risk factors**
W1S1	57	M	HBP

Appendix B. Methodology of *in vivo* measurements

To determine the ascending aorta Peterson modulus and stiffness index for healthy and pathological cases, a standardized protocol using available TEE system (Philips EPIQ7 Ultrasound) with 4–7 MHz multiplane transoesophageal probe was used. Aortic diameters were measured 3 cm above the aortic valve location. Systole was detected by the full opening of aortic valve and end-diastole by the QRS wave peak on the simultaneously registered electrocardiogram. Pressure measurements were performed by sphygmomanometer for the control group and invasively by radial artery cannulation for the dissection group. A mean of two pressure measurements was retained for each patient. The dissection group was composed of patients aged from 50 to 85 years, with aortic dissection involving ascending aorta independently of the entry tear location occurring less than 2 weeks after the onset of symptoms. It is important to note that aortic dissection related to connective tissue genetic disorder (Marfan's or Ehlers-Danlos syndromes), iatrogenic dissection, type A intramural hematoma or dissection occurring in patients with bicuspid aortic valve were excluded of this pathological group. In the control group, patients were selected to match those in dissection group for age and vascular risk factors. They displayed no severe ascending aorta atherosclerosis, aortic-valve disease nor ascending aorta aneurysm.

Appendix C. Tables of results: coefficients of constitutive modelling, R^2 and anisotropy levels

Table C.1 shows C, k_1, k_2 coefficients and γ angle for the mean data obtained from the healthy samples (n = 7), $\overline{Haa}$, and for the only one tested sample of *Daa* wall without dissected layers. $\overline{R^2}$ values obtained during the identification procedure and anisotropy level are also displayed. $Ani_{80} = 2\frac{\lambda_L^{80}-\lambda_\theta^{80}}{\lambda_L^{80}+\lambda_\theta^{80}}$ and $Ani_{120} = 2\frac{\lambda_L^{120}-\lambda_\theta^{120}}{\lambda_L^{120}+\lambda_\theta^{120}}$.

Table C.1
Coefficients of the HGO constitutive modelling, $\overline{R^2}$ values and anisotropy level obtained through the optimization procedure for $\overline{Haa}$, mean data obtained from the n = 7 healthy samples and for *Daa* wall without dissected layers.

	C (kPa)	k_1 (kPa)	k_2	γ	$\overline{R_\theta^2}$	$\overline{R_L^2}$	Ani_{80}	Ani_{120}
$\overline{Haa}$	29.828	10.369	20.93	0.922	0.861	0.811	−0.017	−0.03
Daa wall	13.950	62.056	12.01	0.879	0.902	0.911	−0.025	−0.037

Table C.2
A_{ij} coefficients, anisotropy index and $\overline{R^2}$ values obtained through the optimization procedure for each flap sample and for their mean data.

Flap(F) ID Sample(S) ID	$A_{\theta\theta}$ (kPa)	$A_{\theta L}$ (kPa)	A_{LL} (kPa)	$\overline{R_\theta^2}$	$\overline{R_L^2}$	Ani
F1S1	299.375	111.499	251.451	0.988	0.992	0.174
F1S2	265.494	96.506	212.808	0.978	0.991	0.220
F2S1	293.325	114.408	236.580	0.980	0.976	0.214
Mean data	277.653	114.350	232.861	0.995	0.991	0.175

Table C.2 shows the A_{ij} constitutive modelling coefficients of *Daa* flap samples, the $\overline{R^2}$ values obtained during the identification procedure and the anisotropy level, $Ani = 2\frac{A_{LL}-A_{00}}{A_{LL}+A_{00}}$.

References

Alimohammadi, M., Pichardo-Almarza, C., Agu, O., Diaz-Zuccarini, V., 2016. Development of a patient-specific multi-scale model to understand atherosclerosis and calcification locations: comparison with in vivo data in aortic dissection. Front. Physiol. Comput. Physiol. Med. 7, 238.

Azadani, A., Chitsaz, S., Matthews, P., Jaussaud, N., Leung, J., Tsinman, T., Ge, L., Tseng, E., 2012. Comparison of mechanical properties of human ascending aorta and aortic sinuses. Ann. Thorac. Surg. 93, 87–94.

Babu, A.R., Byju, A.G., Gundiah, N., 2015. Biomechanical properties of human ascending thoracic aortic dissections. J. Biomech. Eng. 137/081013-1.

Deplano, V., Boufi, M., Boiron, O., Guivier-Curien, C., Alimi, Y., Bertrand, E., 2016. Biaxial tensile tests of the porcine ascending aorta. J. Biomech. 49 (10), 2031–2037.

Duprey, A., Trabelsi, O., Vola, M., Favre, J.P., Avril, S., 2016. Biaxial rupture properties of ascending thoracic aortic aneurysms. Acta Biomater. 15 (42), 273–285.

Emmott, A., Garcia, J., Chung, J., Lachapelle, K, El-Hamamsy, I., Mongrain, R., Cartier, R., Leask, R.L., 2016. Biomechanics of the ascending thoracic aorta: a clinical perspective on engineering data. Can. J. Cardiol. 32(1), 35–47.

Golledge, J., Eagle, K.A., 2008. Acute aortic dissection. Lancet 5 (372), 9632.

Haskett, D., Johnson, G., Zhou, A., Utzinger, U., Vande Geest, J., 2010. Microstructural and biomechanical alterations of the human aorta as a function of age and location. Biomech. Model Mechanobio. 9, 725–736.

Hirata, K., Triposkiadis, F., Sparks, E., Bowen, J., Wooley, C.F., Boudoulas, H., 1991. The Marfan syndrome: abnormal aortic elastic properties. J. Am. Coll. Cardiol. 18 (1), 57–63.

Humphrey, J.D., 2013. Possible mechanical roles of glycosaminoglycans in thoracic aortic dissection and associations with dysregulated TGF-β. J. Vasc. Res. 50 (1), 1–10.

Kamenskiy, A., Dzenis, Y., Jaffar Kazmi, S., Pemberton, M., Pipinos, I., Phillips, N., Herber, K., Woodford, T., Bowen, R., Lomneth, C., MacTaggart, J., 2014. Biaxial mechanical properties of the human thoracic and abdominal aorta, common carotid, subclavian, renal and common iliac arteries. Biomech. Model Mechanobiol. 13, 1341–1359.

Koch, R.G., Tsamis, A., D'Amore, A., Wagner, W.R., Watkins, S.C., Gleason, T.G., Vorp, D.A., 2014. A custom image-based analysis tool for quantifying elastin and collagen micro-architecture in the wall of the human aorta from multi-photon microscopy. J. Biomech. 47, 935–943.

Koullias, G., Modak, R., Tranquilli, M., Korkolis, D., Barash, P., Elefteriades, J., 2005. Mechanical deterioration underlies malignant behavior of aneurysmal human ascending aorta. J. Thorac. Cardiovasc. Surg. 130, 677–683.

Labrosse, M.R., Beller, C.J., Mesana, T., Veiot, J.P., 2009. Mechanical behaviour of human aortas: experiments material constants and 3-D finite element modelling including residual stress. J. Biomech. 42, 996–1004.

Martin, C., Pham, T., Sun, W., 2011. Significant differences in the material properties between aged human and porcine aortic tissues. Euro. J. Cardio-thoracic Surg. 40, 28–34.

Matsumoto, T., Fukui, T., Tanaka, T., Ikuta, N., Ohashi, T., Kumagai, K., Akimoto, H., Tabayashi, K., Sato, M., 2009. Biaxial tensile properties of thoracic aortic aneurysm tissues. J. Biomech. Sci. Eng. 4, 518–529.

Okamoto, R.J., Wagenseil, J.E., Delong, W.R., Peterson, S.J., Kouchoukos, N.T., Sundt, T.M., 2002. Mechanical properties of dilated human ascending aorta. Ann. Biomed. Eng. 30, 624–635.

Pasta, S., Phillippi, J.A., Tsamis, A., D'Amore, A., Raffa, G.M., Pilato, M., Scardulla, C., Watkins, S.C., Wagner, W.R., Gleason, T.G., Vorp, D.A., 2016. Constitutive modelling of ascending thoracic aortic aneurysms using microstructural parameters. Med. Eng. Phys. 38, 121–130.

Pham, T., Martin, C., Elefteriades, J., Sun, W., 2013. Biomechanical characterization of ascending aortic aneurysm with concomitant bicuspid aortic valve and bovine aortic arch. Acta Biomater. 9 (8), 7927–7936.

Roccabianca, S., Figueroa, C.A., Tellides, G., Humphrey, J.D., 2014. Quantification of regional differences in aortic stiffness in the aging human. J. Mech. Behav. Biomed. Mater. 29, 618–634.

Roccabianca, S., Ateshian, G.A., Humphrey, J.D., 2017. Biomechanical roles of medial pooling of glycosaminoglycansin thoracic aortic dissection. Biomech. Model Mechanobiol. 13, 13–25.

Shingu, Y., Shiiya, N., Ooka, T., Tachibana, T., Kubota, S., Morita, S., Matsui, Y., 2009. Augmentation index is elevated in aortic aneurysm and dissection. Ann. Thorac. Surg. 87 (5), 1373–1377.

Stefanadis, C., Stratos, C., Boudoulas, H., Kourouklis, C., Toutouzas, P., 1990. Distensibility of the ascending aorta: comparison of invasive and non-invasive techniques in healthy men and in men with coronary artery disease. Eur. Heart J. 11 (11), 990–996.

Thunes, J., Phillippi, J., Gleason, T., Vorp, D., Maiti, S., 2018. Structural modelling reveals microstructure-strength relationship for human ascending thoracic aorta. J. Biomech. 71, 84–93.

Tsamis, A., Krawiec, J.T., Vorp, D.A., 2013. Elastin and collagen fibre microstructure of the human aorta in ageing and disease: a review. J. Roy. Soc. Interf. 10, 20121004.

Vitarelli, A., Conde, Y., Cimino, E., DÁngeli, I., DÓrazio, S., Stellato, S., Padella, V., Caranci, F., 2006. Aortic wall mechanics in the Marfan syndrome assessed by transesophageal tissue doppler echocardiography. Am. J. Cardiol. 97 (4), 572–577.